This is a non-peer-reviewed preprint submitted to EarthArXiv.

Hyperlocal Seismic Soil Characteristic Measurements for Unexploded Ordnance Detection

Barney Gorin — GoVentures, Inc., Gaithersburg, MD; barneygorin@goventures.biz
C. Scott Vaughen — Montgomery County Community College, Blue Bell, PA; csvaughen@gmail.com
Stephen Morehouse — Independent / Retired
Janis Tabor — GoVentures, Inc., Gaithersburg, MD
Paul Kirchman — TerraPower
Joseph Kujawski — Kujawski Consulting, College Station, TX
Patrick McKenna — Independent Consultant
Christopher Kujawski — Texas A&M University, Texarkana, TX

Revisions

Minor revisions such as verbiage changes to implement the revised results and corrections to punctuation errors are not listed.

Rev	Was	Is	Impact
NC	N/A	N/A	First upload to EarthArXiv
1	Accelerometer data squared before normalization	Combined in frequency domain	• Eliminates second-harmonic doubling • Figure 3 peaks move from 200-310 Hz to 100-150 Hz; DC inflation removed • Figure 4 trough near 250 Hz moves to 124 Hz; peaks at 510, 710, 830 Hz replaced by peaks at 360, 550 Hz • Table 2 detection limits recalculated
1	COTS IMU clock step based on initial increment	IMU clock step based on file median increment	Collapsed apparent multiple spikes/troughs into single indications
1	Data reduction ignored steady state background power	Excluded cultural artifacts from data presentation	• Excluded peaks at 409 and 455 Hz from Figure 4 • Removed cultural contamination from attenuation calculations
1	Sod cutter, aluminum angle soil interfaces treated equally	Soil interfaces separated for frequency analyses	Figure 3 redrawn with only sod cutter data
1		Added Table 1	Improved Figure 1, test site information expanded
1		Added Acronym List	Eased understanding of acronyms

This is a non-peer-reviewed preprint submitted to EarthArXiv.

Rev	Was	Is	Impact
2	Figure 4 frequency axis derived from median sample	Frequency axis built from the recorded timestamps	All Figure 4 features move about 2.5% higher
2	Figure 4 trough, peaks	Same features on corrected axis	Trough moved from 124 to 132 Hz, peaks moved from 360 to 372 and from 550 to 564 Hz
2	Narrow 409 & 455 Hz excluded from Figure 4	The two lines at 420 & 466 Hz are reported (Section 4.7)	Reported as strike-driven lines of unknown origin present in a subset of runs; generator attribution shown as part of Rev 1 is withdrawn
2	Spectral differences presented as target-related	Spectral differences cannot be separated from confounds	No target detection claimed
2	Near-130 Hz change described as target-related	Near-130 Hz change identified at both sites	Came from comparing different sensors, mounts or positions. Same-sensor comparisons show larger changes for nearer targets; these cannot be separated from time, so a target effect cannot be stated as a firm conclusion.
2	Figure 4: difference of no-target and with-target averages	Figure 4 replaced: one sensor at one fixed position, one no-target and three with-target runs	The original runs came from sensors at different positions.
2	Table 2 minimum detection dimensions	Recomputed	548 changed to 515 mm; 189 changed to 183 mm; 124 changed to 121 mm
2	Bally Cliff peak at 129 Hz, trough at 133 Hz	Trough at 131 Hz, peak at 168 Hz	Bally pattern came from pooling two sensors on two mount types; not the same feature as at BCDC

This is a non-peer-reviewed preprint submitted to EarthArXiv.

Peer review status:

This is a non-peer-reviewed preprint submitted to EarthArXiv. It has not been submitted to a peer-reviewed journal.

Hyperlocal Seismic Soil Characteristic Measurements for Unexploded Ordnance Detection

Barney F. Gorin, PE, C. Scott Vaughen, Stephen Morehouse, Janis Tabor, Paul Kirchman, Joseph Kujawski, Patrick McKenna, Christopher Kujawski

Abstract

Explosive Remnants of War (ERW) range from small plastic landmines to unexploded cannon shells to bombs that weigh hundreds of kilograms. They kill and maim thousands of people each year, make otherwise productive real estate unusable, and exist worldwide. Their variability and the variability of the soil in which they exist defeat and delay cleanup efforts.

Current search technology treats soil as a problem or nuisance variable.

We propose to measure soil properties hyperlocally (meter by meter) with a foundational approach that exploits broadband seismic stimulus and commercial off the shelf (COTS) instrumentation to characterize detection capability in site-specific soil context.

Field experiments were conducted at three widely spaced locations, with data from four soil types at two of them reported here, to research the feasibility of hyperlocal seismic measurements that include P-wave velocity, attenuation, and frequency content.

Spectral changes between no-target and with-target runs were observed at two independent test sites, but on close analysis none could be cleanly attributed to the ad hoc targets: at Bally Cliff because of two different sensors on two mount types, and at BCDC because the sensors were at different positions. Comparing each sensor to itself, each site shows a larger change for the nearer target positions, but at both sites those runs were recorded later than the no-target runs, so a target contribution cannot be stated as a firm conclusion. What the data do establish is that real, meter-scale soil response can be measured with COTS instrumentation. These preliminary results indicate that soil-adaptive detection using soil characterization as the primary data layer rather than an afterthought offers a path toward safer, more predictable, and more efficient ERW clearance operations.

We conclude that further research into this technology is needed.

1 Introduction

1.1 The Scale of the Problem

We are under no illusions about the scope of the unexploded ordnance (UXO) problem. In the United States alone, "*The UXO cleanup problem … 10 million acres of land at some 1400 sites. Estimated clean-up cost of … tens of billions of dollars. … instruments that can detect the buried UXOs also detect numerous scrap metal objects and other artifacts*". While things have improved since 2003, the Defense Science Board's assertion that "*Typically 100 holes may be dug before a real UXO is unearthed! …*" remains too close to reality [1].

We are under no illusions about the human cost of UXO and landmines. According to Landmine Monitor 2025 [2], landmines and ERW killed at least 1,945 people, injured 4,325, and left nine with unknown outcomes in 2024. Eighty-six percent of those 6,279 people were civilians and children made up forty-six percent of civilian casualties where the casualty's age was included in the report.

We are under no illusions about the breadth of the UXO and landmine challenge. According to "To Walk the Earth in Safety 2023" [3], 31 African nations, 12 East Asia and Pacific nations, 19 European nations, 10 Middle East and North African nations, 9 South and Central Asian nations, and 13 Western Hemisphere nations other than the United States were actively engaged in ERW cleanup activities.

Ninety-four nations worldwide.

We are under no illusions about the trajectory of this threat. One need only read the headlines about wars—the Russia-Ukraine war, conflicts in the Middle East—to know that the challenge is growing rather than decreasing.

We are under no illusions about the methodology available to detect ERW. It is directly tied to human effort: one person, one detector, possibly operating in an organized group. This is an artisanal process akin to the hand loom weavers who produced cloth before the Industrial Revolution.

We are under no illusions about the availability of bombs and cannon shells and landmines. The means to manufacture and distribute the weapons systems that become ERW advanced into the industrial age in the mid-nineteenth century or almost 200 years ago. Given the artisanal versus industrial competitive landscape, it is little wonder that the scale of the ERW problem is increasing.

- **Technology.** Threat detection technology focuses on the common characteristic of unexploded ordnance and landmines of a quarter century ago: metal. Metal detectors and magnetometers, each operated by a single human, are the site search state of the art. Other detectors, such as ground penetrating radar (GPR) are also human operated.
- **Trained Animals.** Dogs and rats have been trained to search for subterranean threats. While they offer a different sensing system than the metal detectors, a different technology, the one human to one detector ratio remains constant.
- **Trained Humans.** It is not uncommon for sappers to search for ERW using the least sophisticated of all technologies, a simple probe with which to search beneath the surface of the Earth.

We are under no illusions about the challenge of the environment in which ERW is hidden. Soil is incredibly complex and variable. The hyperlocal mixture of sand, clay, and silt varies rapidly in the three obvious dimensions of north-south, east-west, and up-down. Its moisture content and temperature can vary in hours as the sun warms the surface and in minutes as rain adds water. Its chemistry is also complex as, for example, volcanic soils often have very high iron content. Life changes the soil with root structures and tunnels. War changes the soil with a variety of metallic debris, only a small part of which remains a hazardous explosive device.

1.2 Current Approaches and Their Limitation

One size cannot fit all nor can one technology. Every detection technology—electromagnetic, acoustic/seismic, magnetic—propagates energy through soil. The soil's hyperlocal properties determine how that energy travels, attenuates, reflects, and scatters. And how it returns information to that technology's user.

The underlying mathematics is simple: the minimum directly detectable object size is proportional to the wavelength; the maximum detection range is determined by the remaining wave energy at the sensor. Both depend entirely on soil properties that can vary over a meter or an hour.

These are not minor calibration issues. In a seismic technology example, laboratory-measured propagation speeds range from 86 to 260 m/s across soil types and moisture conditions; attenuation varies by orders of magnitude [4]. Moisture absorbs GPR's microwaves. Laterite confounds detectors focused on magnetism and metals. These factors so limit the effectiveness of electromagnetic and mechanical search technologies that, as described above, trained dogs and rats remain in service today.

In some cases, incremental improvements have been achieved. Modern sensor fusion approaches such as the AN/PSS-14 Mine Detection System, magnetometer arrays, and towed multi-sensor platforms have made incremental improvements in detection range and target discrimination. In other cases, progress has been elusive. For example, seismology using acoustic-to-seismic coupling [5, 6] and nonlinear soil-mine resonance [7] has been shown to work well in controlled conditions but could not achieve reliable performance across varying soil types and field environments.

The limit these approaches share is their view of the soil and its place upon the Earth. In some cases, it is a nuisance variable to be overcome. In others it is a fixed parameter. Sometimes it is information to be "looked up" as a reference.

This view of the medium in which the search is to be conducted, a foe rather than a friend, is the common thread.

1.3 The Proposed Shift: Soil as Partner

We propose a fundamental shift in how the soil is viewed: it is a friend and colleague in the search for ERW rather than a foe or a nuisance. It is the primary data layer on which all sensor data is interpreted. It is an informant that, coaxed to do so, will reveal a great deal about what it is and what it holds.

This paper reports on field experiments testing the feasibility of recording seismic waves, and measuring the P-wave propagation velocity and frequency, using hyperlocal COTS

instrumentation. It further reports on whether those waves have frequencies and are traveling at velocities that can support the ERW detection mission.

Based on these test results, we propose using broadband rather than forced frequency stimulus and hyperlocal, i.e., meter by meter, near real-time wideband sensing to let the soil answer us in its own way, to reveal what it is willing to reveal.

And it is willing to reveal quite a lot. The work reported here is an early feasibility demonstration of that proposition, a first look at whether the measurements are achievable with simple equipment, not a complete characterization of the soil at each site.

2 What We Measure: Six Hypotheses

The seismic subsurface object location technology described in this paper rests on six hypotheses that are based on a foundational observation: real soil, when excited by a broadband impulse, contains and transmits seismic energy at frequencies high enough to be compatible with detecting objects of ERW scales. The field experiments reported here include measurements of energy near 900 Hz in the IPG CLAY facility and from 800 to 1,100 Hz at Bally Cliff Farm.

The first four of these hypotheses address specific gaps in the soil property data that have prevented effective use of seismic technology for ERW detection [4]. All the measurements are made of hyperlocal, i.e., meter by meter, soil properties using simple, COTS instrumentation.

Hypothesis 1: It is possible to measure P-wave velocity, which is the most conservative approach to calculating the sensitivity of ERW location using seismic technology.

Hypothesis 2: It is possible to measure seismic frequency content, which is the second key variable in calculating ERW location sensitivity.

Hypothesis 3: It is possible to use the seismic frequency content from Hypothesis 2 to calculate the temporal attenuation coefficients for each seismic frequency. This determines the minimum time between stimulus events and the time during which useful data may be acquired after each event.

Hypothesis 4: It is possible to use the seismic frequency content from two sensors at known relative positions as obtained under Hypothesis 2 to calculate the spatial attenuation coefficients for each seismic frequency. This information describes the potential instrument sensing range.

Hypothesis 5: It is possible to use the hyperlocal seismic wave frequencies and velocities to calculate the smallest object detectable through frequency shifts within range of a sensor. This is the critical performance criterion for an operational ERW detection system.

Hypothesis 6: It is possible to use the hyperlocal seismic waves to detect a change in the nearby soil's hyperlocal properties that indicate a soil anomaly. Such anomalies are likely to indicate the presence of an object that cannot be detected directly.

We note that inadequate sample rates have a major effect on successful seismic measurements as discussed in Section 4.2.

3 Technical Approach

3.1 Methodological Foundation: Let the Soil Speak

This approach originated from a first-principles analysis of seismic instrumentation for a lunar regolith characterization concept that some of the coauthors supported. Applying the calculations involved to the challenge of detecting subsurface terrestrial objects seemed simple enough.

3.1.1 Initial Testing at the Brady Residence

The first principles calculations led to a recognition that the wave frequencies below 100 Hz, even for the slower wave types, would be of limited value in a search for most ERW sized objects. Discussions among the coauthors and preliminary investigations into the literature describing soil frequency response, seismic wave velocities, and energy attenuation [4] led to a very informal test series focusing on what, if any, frequencies of interest might be found and how far such frequencies might propagate. Further coauthor discussions identified a low-cost, high-frequency COTS inertial measurement unit (IMU) instrument and evaluation kit for a single channel data acquisition (DAQ) approach and the owners of a convenient site were willing to support the effort by donating the use of their property.

3.1.2 Test Procedure Development and Data Acquisition at Bally Cliff Farm

The Brady Residence experience led to several general changes in test procedures. The most important of these, adding a multi-channel DAQ for simultaneous data acquisition from multiple IMUs with a common time reference, failed unexpectedly when we attempted to implement it on July 9.

Testing resumed on August 7 using the two single channel DAQ systems as the multi-channel DAQ remained inoperative despite a continuing software development effort. This test series occurred on August 7, 8, 11, and 12 in a small copse of trees on Bally Cliff Farm. The results of those tests, described in Section 4, established the methodological foundation for subsequent testing at the Bush Combat Development Complex (BCDC) Innovation Proving Grounds (IPG).

The test procedure changes implemented at Bally Cliff included:

1. The addition of a second single channel DAQ
2. A "whack it and wait" stimulus strategy to allow the soil to respond in its own way
3. A down select on surrogate sensor to soil interface hardware
4. The addition of targets, seismic ERW simulants, for some runs
5. The addition of more distant sensor positions.

3.1.3 Multi-soil Testing at the Bush Combat Development Complex

The stimulus cycles developed at Bally Cliff Farm were fully implemented at approximately 0.5 Hz based on success using that cadence. The test instrumentation and DAQ configurations were adapted to the exigencies of actual test operations as described in Section 4.1.3.

3.2 Detection Geometry: Volume vs. Area

The scope of the ERW problem is often expressed in terms of the area of the soil's surface, square meters or kilometers, that is affected. This is misleading because the issue is volumetric. Landmines covered by centimeters of soil are a different problem than unexploded bombs several meters below the surface. This difference in characteristics slows down ERW clearance by requiring a search for suspected landmines to be completed before a search for unexploded ordnance can begin [12].

Our operational concept addresses this in a way that is fundamentally different from conventional seismic survey methods. Rather than a single sensor or linear array that is repositioned sequentially across a site, we deploy sensors continuously in an evolving two-dimensional array. Each sensor position contributes to the coverage volume immediately upon deployment. Low-energy automated stimulus allows data acquisition to proceed exactly where it is needed as the array grows. Sensor spacing is adapted to measured hyperlocal soil conditions: sensors are closer together where attenuation, detection requirements, or imaging objectives demand, wider apart where soil conditions and threat characteristics permit.

The robotic deployment strategy that is a fundamental building block of our approach allows coverage rates to scale rather than be constrained by the pace of human operations. Near real-time data processing for key parameters allows robot path replanning as needed for safe operations and to maintain productivity.

Surface coupled sensors such as handheld magnetometers and GPR, are used to search an area defined by their footprint and the ribbons of soil they examine as the sensor moves. This requires careful, systematic surveys with the sensor's path precisely controlled because gaps lead to unexamined volumes while overlaps are merely duplications of prior results. The search volume is the area of the ribbon of soil searched and the sensor's ability to penetrate the soil being examined, which is driven by hyperlocal soil conditions that are often unknown.

Seismic sensing can offer significant advantages, especially for initial survey operations.

Seismic searches are volumetric with hemispherical search volumes. The research reported here indicates that seismic energy propagates usefully for distances exceeding 5 m in favorable soil conditions. This suggests effective search volumes on the order of hundreds of cubic meters for a single source/sensor combination may be possible depending on the hyperlocal soil characteristics. Overlaps in this volume from closely spaced sensors are not duplicative, they are complementary because the energy's path from the stimulus to the object and from the object to the sensor varies, which produces additional knowledge.

The spectral analysis reported here operates on temporal signals at individual sensor positions and does not require spatial phase coherence across the array. Therefore, the sensor spacing does not limit the detectable frequency content; that is constrained by the temporal sample rate of the individual sensor. The planned operational system deploys sensors at spacings determined by measured, hyperlocal soil properties. This allows the spatial sampling density to be adjusted as needed to address productivity or needed analysis inputs as conditions require.

Importantly, measuring the hyperlocal spatial attenuation of the seismic energy for each frequency in near real-time during the search allows the detectable object size to be known as a function of distance from the sensor, rather than assumed based on reference data. This allows

the seismic source and detector array to be optimized for both productivity and efficacy in the expected threat environment and simplifies automated emplacement.

3.3 Multi-Physics Convergent Evidence

Our seismic sensor platform is expected to provide sufficient size, weight, power, and data resources to accommodate other sensors. Several orthogonal sensing technologies have been examined, and notional configurations have been developed for some. We plan to incorporate a selected orthogonal technology in next-generation test hardware, but no detailed designs, strawman hardware configurations, or test articles have been developed.

Seismic sensing is an attractive candidate for multi-physics sensor fusion because it is an acoustic impedance phenomenon while most detectors are based on magnetic, electromagnetic, or electromagnetic radiation physics. Magnetometry senses the magnetic fields associated with ferromagnetic materials. Metal sensing uses transmitting and receiving coils to detect eddy currents that result from the presence of conductive materials such as metal. Both are orthogonal to seismic phenomena, so fusing either of them with seismic sensing would bring information from disparate physics. Multi-sensor fusion that combines orthogonal physics has been shown to improve detection probability and reduce false alarm rates in UXO applications [9].

Similarly, soil characterization provides important information for electromagnetic technologies operating on separate platforms. Hyperlocal soil characterization can include moisture data to indicate the likely GPR signal penetration depth [13], since soil moisture is a primary factor governing GPR attenuation. Seismic area searches can also identify specific anomaly locations that are appropriate for detailed investigations with orthogonal technologies such as GPR.

4 Field Experiments and Results

4.1 Test Sites and Instrumentation

Tests were performed at three sites: the Brady Residence in Pennsylvania; Bally Cliff Farm in Maryland; and the Bush Combat Development Complex in Texas as shown in Figure 1. Testing took place over the two-month period beginning on June 23, 2025, and ending August 21, 2025 [14].

Figure 1. Test locations were dispersed over a wide geographical area.

The conditions at the test sites are summarized in Table 1

Table 1. Test sites.

Site	Location	Nature	Soil type	Dates (2025)	Distances (m)	Coupling
Brady Home	Enon Valley, PA	Exploratory	Unknown (not included in soils tested count)	June	Varied	Varied
Bally Cliff Farm	Poolesville, MD	High data rate	USDA Web Soil Survey data • Penn silt loam • 3 to 8 percent slopes • Topsoil thickness not measured • Typical values for Penn series A horizon are 10 to 25 cm over silt loam B horizon	June-August	3, 5, 5.9, 7	SC + AA
BCDC CLAY	Bryan, TX	High data rate	100% clay, 0.9 m depth over 200 mm concrete	Aug 20–21	1, 2, 3, 4, 5, 6	SC
BCDC SAND	Bryan, TX	Low data rate	100% sand, 0.9 m depth over 200 mm concrete	Aug 21	1, 2, 3, 4, 5, 6, 7	AA
BCDC NATIVE SOIL	Bryan, TX	Low data rate	USDA Web Soil Survey data • Silawa fine sandy loam • 2 to 5 percent slopes	Aug 21	1, 2, 3, 4, 5, 6, 7	SC

The general test geometry consisted of a seismic source and a series of IMUs arranged along a single axis as illustrated in Figure 2. The grid is shown as 2 m squares, but the sensors were arranged at 1 m spacing for many tests. Similarly, while the simulated targets are shown at both + and -y locations, testing was generally conducted with the target at a +y position for convenience and because the arrangement was generally symmetrical about the x-axis centerline.

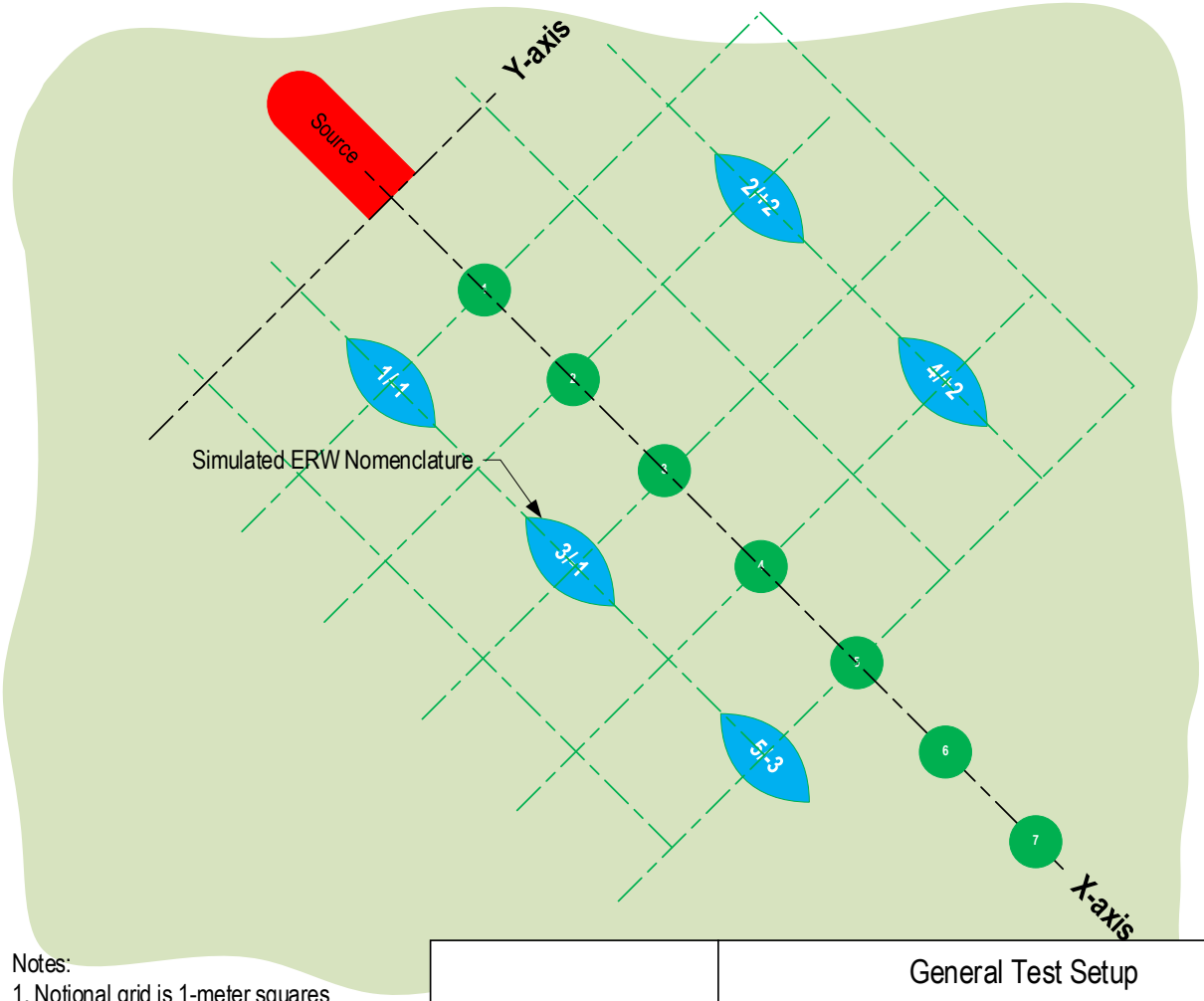

Figure 2. Typical seismic stimulus source, IMU, and simulated ERW locations.

Two primary instrumentation systems were used: a microelectromechanical systems (MEMS) IMU that delivered three-axis accelerometer data; and a contact microphone that provided a single energy level output. Each of these instruments was mechanically coupled to the soil using surrogate tooling.

Three data acquisition systems were used: a dedicated ST MEMS evaluation/adapter board sold by the IMU manufacturer; a COTS DAQ designed to support 8 independent instrument channels; and a recording oscilloscope supporting 2 contact microphone channels.

The seismic stimulus energy ranged from 3 to 6 joules at stimulus frequencies from 130 to 0.5 Hz. This energy is compatible with automated delivery mechanisms.

4.1.1 Brady Residence Testing

Testing at the Brady Residence in Enon Valley, Pennsylvania took place on June 23 through 25, 2025. The primary work included test setup experiments, testing tooling concepts, observing general test results, and examining a variety of test site characteristics. Digital data was acquired during six test runs.

A motorized hammer operating at ~130 hammer impacts per second was used based on the assumption that a controlled-frequency stimulus would produce an interpretable soil response at a frequency high enough to be of value. Instead, the continuous stimulus flooded the soil with overlapping signals. This finding led to the subsequent use of the broadband impulse seismic stimulus methodology. A conservative view of the soil's attenuation characteristics led to limiting planned testing to sensor distances from the stimulus of ~0.5, 1, 2, and 3 m.

This early test series validated the selection of the MEMS IMU as a primary sensor.

4.1.2 Bally Cliff Testing

A COTS DAQ able to acquire multiple COTS IMU channels appeared to be functional during software development but failed to operate in the field on July 9 and no data was taken. Testing was suspended at that point in the hope that the DAQ issues could be resolved. The DAQ issues proved to be more difficult to resolve than expected and testing resumed on August 7, 2025, with the two parallel COTS ST MEMS evaluation/adapter board data pipelines.

Testing at Bally Cliff Farm in Poolesville, Maryland, took place between August 7th and August 12, 2025.

The testing was generally performed in a copse of trees penetrated by farm lanes connecting three fields. The soil in the test area was not examined beyond general observations but is believed to be a combination of organic material, silt, and loam with substantial subsurface organic material such as tree roots throughout.

In addition to tests designed to measure soil characteristics, shovel points inserted in the soil as surrogate ERW items, or targets, were included in the testing. A total of 35 runs (24 no-target, 11 with-target) were conducted with sensor distances of 3 to 7 m from the seismic energy source. Two no-target runs were excluded from the spectral analysis for the data-quality reasons described in Section 4.4, leaving 22 no-target runs in that analysis.

The whack it and wait stimulus strategy was put into practice. Listening to the soil's response to a broadband stimulus rather than interrogating it at predetermined frequencies [5, 6, 7, 8] provided data useful for ERW detection.

4.1.3 Bush Combat Development Complex Testing

The BCDC IPG contains designated test areas identified as CLAY and SAND named for the soil type in each facility. We adopted the BCDC capitalization structure to identify our NATIVE SOIL test location adjacent to SAND.

The BCDC test plan was based on full multi-channel DAQ availability at the beginning of testing. It was baselined as an intense one-day effort with multiple sensor locations along a single

axis in each BCDC location. With those tests complete, a series of shovel points as ERW simulants were to be added at various positions.

A total of 39 runs were conducted including 3 unofficial "setup" verification tests. Seventeen of these runs, including the 3 setup runs, were conducted in CLAY, 16 in SAND, and 6 in NATIVE SOIL. Fifteen runs included ERW simulants.

CLAY and SAND are homogeneous layers of the stated soil in a constrained pit approximately 27.5 m (90 ft) in diameter and 0.9 m (36 in) deep. The NATIVE SOIL was not examined in detail but is generally believed to consist of acidic sandy loam, loamy fine sand, some gravel, and limited organic material.

Despite expectations about its availability and ability to provide data acquisition rates above 2 kHz range, the multi-channel DAQ was not available on the first day of testing.

The two single-channel IMU-DAQ systems were set up in the CLAY facility and testing began at a much-reduced cadence on August 20 with the stimulus cycles targeted to be at 0.5 Hz.

Testing continued on the 21st. A contact microphone and digital data logger, a third instrumentation-DAQ option, were added for some testing in CLAY to partially address the difficulties with the multi-channel DAQ. Testing began in SAND with the multi-channel DAQ. Despite manufacturer's literature performance specifications, it was only able to support 6 data channels at a data acquisition rate slightly above 300 Hz.

The multi-channel DAQ system and instrumentation were moved to NATIVE SOIL when the runs planned for SAND were completed. A weather event forced an early end to test operations.

4.2 The DAQ Lesson

Multi-channel data acquisition at the Texas test site relied on COTS interface hardware that could not meet performance expectations based on manufacturer literature. The resulting effective sample rate of slightly over 300 Hz—versus the above 2 kHz sample rate achieved with the single-channel ST MEMS evaluation/adapter board DAQ—all but eliminated useful frequency content at the SAND and NATIVE SOIL test areas by reducing the Nyquist frequency to approximately 150 Hz. Coarse P-wave velocity estimates may be possible from arrival-time analysis, and analytical work to recover them is ongoing, but the desirable spectral characterization of these soil types will require retesting with adequate data acquisition equipment.

This experience confirmed that data acquisition bandwidth is not a peripheral concern but a first-order system requirement for hyperlocal seismic characterization. The design of, and planning for a purpose-built, widely expandable, Raspberry Pi-based DAQ with GPS-synchronized timing is underway to address this limitation in planned future testing.

4.3 P-wave Velocity

P-wave velocity was measured as 272 m/s in BCDC IPG CLAY using two contact microphones separated by 3 m, a digital oscilloscope acquiring data from them at 10 kHz, and first-break picking on the recorded waveforms. An initial high-frequency arrival consistent with propagation at atmospheric acoustic velocity (about 343 m/s) was identified and disregarded. At 3 m separation, the air-coupled wave precedes the soil P-wave by approximately 1.8 ms and is

distinguishable by its frequency content (approximately 3 kHz) and propagation speed. Subsequent digital analysis of this data produced a P-wave velocity of 286 m/s. These values are both very similar and slightly above the high end of the P-wave velocity range Oelze [4] reports, i.e., from 86 to 260 m/s, across soil types. The 272 m/s P-wave velocity is used in the detection limit calculations in Section 4.8 because the visual interpretation of the wave was believed to be more reliable than a software script interpreting very limited data.

Data analysis is continuing for the lower bandwidth data acquisition system used in the BCDC SAND and NATIVE SOIL locations. An ad hoc synchronization of the two single-pipeline, high-bandwidth instruments has since given a CLAY surface-wave velocity of 159 ± 9 m/s (Gorin et al., in preparation). This work will continue and be reported as a part of future research.

4.4 Frequency Content and Spectral Characterization

Coherent seismic signals were recovered at sensor distances of 3 to 7 m from a bulkhead/bang-plate source at Bally Cliff Farm during testing on 7 and 8 August 2025. Twenty-two of the twenty-four candidate runs, none of which included a reflector target, were used in the present analysis. Two runs were excluded: August 7 Run 3A, whose data file is below the processing pipeline's minimum-size threshold, and August 8 Run 13, which the field log flags for bad spikes. Each run captured approximately six hammer-strike stimulus events (median 6, range 2–8 across the runs used). Per-blow power spectra were averaged within each run and run-mean spectra were further averaged across the runs at each distance (twenty-two runs total: 7, 10, 3, and 2 at 3, 5, 5.9, and 7 m respectively). Averaging power spectra reduces the variance of the spectral estimate in proportion to the number of averages; it does not lower the mean noise level, so the floor visible in Figure 3 is the noise floor of the measurement itself.

Sensor coupling to the soil was through one of two interface plates: a sod-cutter (SC) blade or an aluminum-angle (AA) bracket with the MEMS sensors attached. The single channel data acquisition connection was moved from sensor to sensor between recording sessions.

A mount-comparison experiment performed at the same site on 11 August 2025, with simultaneous dual-channel recording on co-located sensor pairs with one SC and the other AA using two parallel single-channel data acquisition connections, showed that the two mountings agree to sub-millisecond vertical timing and within ±5% on vertical amplitude after gravity-frame alignment of each sensor (Gorin [16]). That validation is limited to vertical timing and amplitude; it did not establish spectral-shape equivalence, and the same experiment observed reduced vertical-axis coherence in the 50–150 Hz band for mixed-mount pairs (median 0.53, versus 0.80 for same-mount pairs). Consistent with that caution, the present dataset shows distinct dominant frequencies for the two mountings at the 3 m position: approximately 130 Hz in the sod-cutter no-target runs (n = 5) versus approximately 152 Hz in the aluminum-angle no-target runs (n = 2).

The two mountings are therefore not pooled for spectral analysis. Figure 3 presents the sod-cutter runs, which form the larger and more evenly distributed sample (n = 5, 6, 2, and 1 at 3, 5, 5.9, and 7 m). The aluminum-angle runs are retained for amplitude- and timing-based analyses, to which the mount-equivalence validation applies.

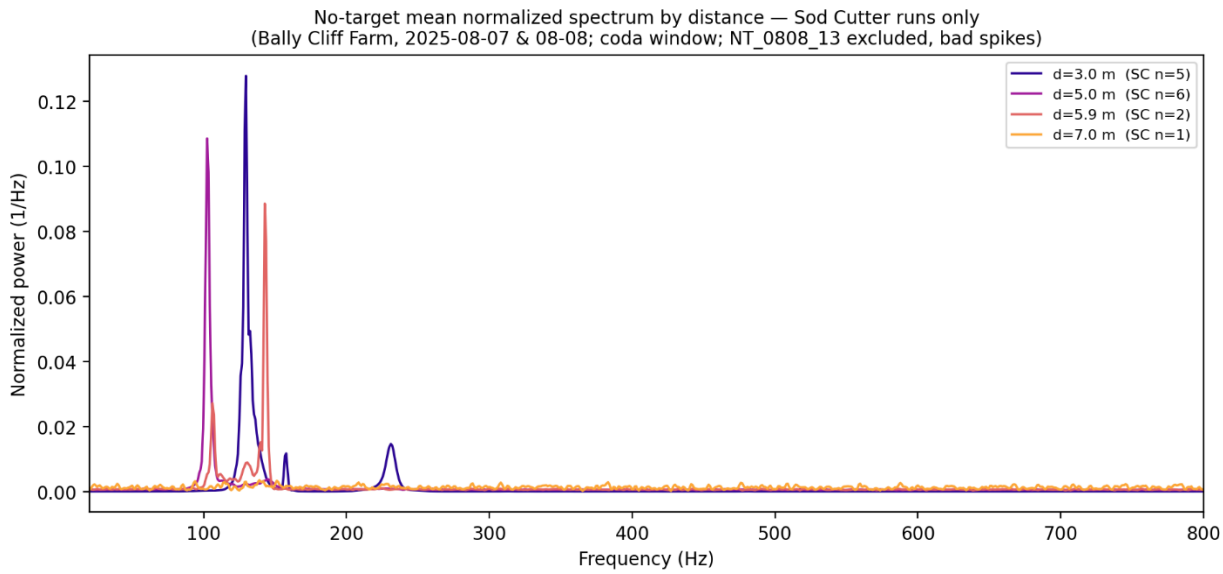

Figure 3. Run-mean spectra by sensor distance at Bally Cliff Farm (sod-cutter runs).

The sample size shown in Figure 3 is the number of sod-cutter runs at each distance during the test series.

We note two observations about the data shown in Figure 3.

Instrument noise floor. Above approximately 250–350 Hz the recorded spectra at Bally Cliff Farm lie at the instrument and ambient noise floor at all four distances, including the closest (3 m): coda-window band power at 250–400 Hz and at 400–700 Hz is independent of distance and lies within approximately 4 dB and 1 dB, respectively, of same-duration pre-event noise windows. The dataset therefore places no constraint on frequency-dependent attenuation by this measure, which is nonetheless expected in unconsolidated soil (Oelze [4]). This limit is a property of the coda-averaged spectrum used here, not of the data; the high-frequency arrivals it averages out can be recovered by other processing, which we take up elsewhere (Gorin, DSIAC Journal, in press). In the normalized display of Figure 3 the weakest spectrum (7 m) exhibits the highest apparent floor; this is an artifact of normalization, not high-frequency energy surviving to that distance.

Peak structure versus distance. The 3, 5, and 5.9 m distances each exhibit a narrow-band spectral peak in approximately the 100 to 150 Hz range (129.6, 102.4, and 142.7 Hz respectively); at 7 m the corresponding feature is approximately 2 dB above a same-duration noise window and is reported as marginal. The per-axis combination places the dominant peaks in the 100 to 150 Hz range. Because the spectra in Figure 3 are normalized, differences in peak height reflect spectral concentration rather than absolute amplitude, and spatial attenuation cannot be read from this figure; source amplitude was additionally uncontrolled, with runs at the same position minutes apart differing by an order of magnitude in 100–150 Hz band power. We therefore report only that a low-frequency spectral peak is present at the three well-sampled distances, and we identify a controlled re-test with balanced sampling as necessary to establish whether the peak frequency varies systematically with distance or with position on the site.

The sample size shown in Figure 3 is the number of runs with the sod cutter sensor mounting system at each distance during the test series. The sample size is the total number of runs at each distance.

The site is a linear clearing where three farm lanes converge in a copse of trees that may include tree roots, animal burrows, and other small-scale heterogeneities. The testing took place over two days. The bulkhead and instrumentation were removed at the end of the first day and reinstalled in a nearby location the next so that the distances were measured along slightly different paths through the medium. The spectra may therefore differ between the two days' paths.

The controlled mount-comparison experiment of 11 August 2025 (Gorin [16]) addresses one specific subset of this question—whether mount type alone produces measurable differences in the recorded vertical motion—and finds no significant mount effect on either amplitude or timing at the ±5% / sub-millisecond level. Disentangling the remaining contributors will require simultaneous dual-channel recording during identical stimulus events at multiple distances, an experiment that was not part of the present test series.

Limited statistical power at 7 m. The 7 m result rests on n = 1 run and supports no quantitative conclusion about the spectrum at that distance. The small excursion above the noise floor near 140 Hz on the 7 m trace is a feature of that specific run and should not be over-interpreted.

4.5 Temporal and Spatial Attenuation

Both temporal and spatial attenuation vary with soil type and condition, e.g., moisture content. Reference or average values are insufficient for ERW detection through seismic operations as a result. We believe that real-time hyperlocal seismic data analysis can mitigate this difficulty and data supporting our thesis through attenuation measurements was acquired at Bally Cliff Farm and in the IPG CLAY facility.

We calculate temporal attenuation using an exponential fit to the Hilbert envelope of narrow-band-filtered records and report the median across the three axes such that it does not depend on a cross-axis combination.

Because the analysis bandwidth imposes a ceiling on the measurable decay rate, the values reported here use a 20 Hz filter half-width, with each fit terminated where the envelope approaches the ambient noise level. At Bally Cliff Farm the decay rate (s^{-1}, or Alpha) is structured by frequency: energy at each sensor position's dominant frequency decays at approximately 12 to 18 s^{-1} with a decay time, or Tau, of approximately 55 to 85 ms. Energy at nearby frequencies but not at that peak decays roughly twice as fast, at approximately 25 to 40 s^{-1}. In the CLAY facility, low stimulus amplitudes in some runs and sensor overload in others constrain the measurement to a range of approximately 17 to 44 s^{-1} at 140 to 180 Hz, so we do not report a single CLAY value. Fitted values in the 380 to 550 Hz band at CLAY are excluded entirely: the lightly damped 420 and 466 Hz lines (Section 4.7) ring longer than the surrounding coda and bias fitted decay rates toward zero.

Spatial attenuation varies with frequency. Below approximately 250 Hz, near/far amplitude ratios at CLAY indicate spatial attenuation of order 10 to 20 dB/m. We do not report values at higher frequencies, where the ratios are affected by the same narrowband lines (Section 4.7) and, above approximately 600 Hz, by the instrument noise floor. We treat the reported magnitudes as

indicative only because the near and far records came from different sensors and differ in spacing between runs, the stimulus amplitude was not controlled, and the run-to-run scatter is too large to claim precise attenuation values.

4.6 Soil-Type Spectral Differences

Wave spectral responses were successfully developed for the Bally Cliff Farm and in the IPG CLAY facility, both with and without surrogate targets located at various distances normal to the line through the seismic source and sensor positions.

Spectral differences between no-target and with-target runs were observed at both sites near 130 Hz, and at both sites the difference takes the same form: a trough at one frequency paired with a peak immediately beside it. At BCDC the trough is near 132 Hz with a peak near 147 Hz; at Bally Cliff the trough is near 131 Hz with a peak near 168 Hz. At Bally Cliff the with-target set pooled two sensors on two mount types (sod cutter and aluminum angle), while every no-target run came from the sod-cutter sensor; the paired dip and rise comes entirely from the aluminum-angle runs. The sod-cutter sensor alone shows no difference beyond its run-to-run spread when the target was 3 m off the line; with the target 1.5 m off the line (the last two runs) its ringing differed by two to three times the run-to-run spread, which cannot be separated from time, so a target contribution cannot be stated as a firm conclusion. At BCDC the no-target and with-target recordings came from sensors at different positions, which most likely produces the same pattern there.

In a “like to like” comparison, the 3 m no-target Bally Cliff Farm and the 3 m no-target IPG CLAY data show clearly different spectral shapes. This difference is a demonstration of the importance of hyperlocal soil characterization data.

4.7 Target (ERW Simulant) Detection: Preliminary Observations

Testing included runs with and without a target, or ERW simulant, at both Bally Cliff Farm and at BCDC. The Bally Cliff Farm and BCDC IPG CLAY data were taken at a high data rate while the SAND and NATIVE SOIL data were taken at slightly more than 300 Hz.

Hand shovels were used as metallic targets rather than high-fidelity ERW simulants. They were forced into the soil to convenient depths and not dimensionally characterized during testing. A lesson learned is that future experiments will use targets of known dimensions to enable direct comparison with calculated detection limits.

A note handwritten on the BCDC run log states “Target runs have overload on S waves for max def on P waves.” The sensor used in Figure 4 did not overload.

Figure 4 compares coda spectra recorded by one sensor at one fixed position in the BCDC CLAY facility, about 3 m from the source: one run without a target and three runs with targets at two positions. The spectra are computed from the coda, 50 to 300 ms after each first break, with 10 ms end tapers, and each blow is normalized over 20 to 780 Hz before averaging. The pre-strike background is shown for reference. The amplitude spectra for the three sensor axes (vertical and two horizontal) are computed independently via FFT, then combined as the square root of the sum of squared per-axis spectra at each frequency. The analysis window includes all the wave energy present at the sensor. No wave-type separation has been applied. The spectral differences shown reflect the aggregate response of the soil-target system to broadband excitation.

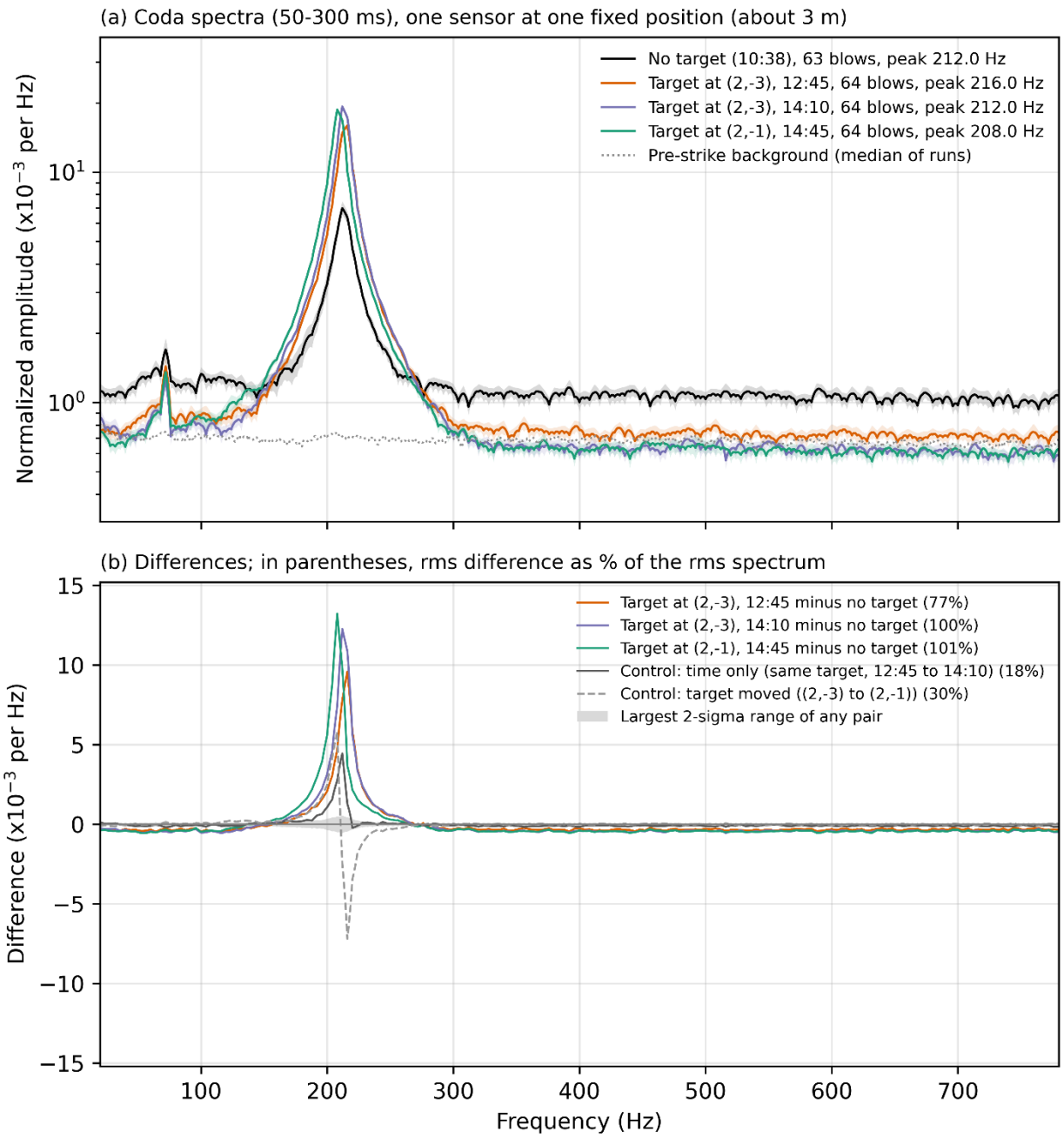

Figure 4. BCDC IPG CLAY coda spectra from one sensor at about 3 m from the source: one run without and three runs with ERW simulants.

In Figure 4, the three with-target runs differ from the no-target run by 77 to 101% (rms difference relative to the spectrum), against 18% for the same target 85 minutes later and 30% when the target was moved. No-target repeat runs on two other sensors differ by 11 to 33%. Most of the difference is a broadband floor and a weaker ring near 210 Hz in the no-target run. A target contribution cannot be separated from conditions in the no-target run, the only one at this sensor and the first after installation. At the 2 m sensor that run also differs more from the next run (33%) than later runs differ from each other (17%). The broad peaks near 372 and 564 Hz

are real, hammer-driven soil energy, strongest at the sensor about 1 m from the source and are probably a feature of that position.

Two narrow spectral lines, near 420 and 466 Hz, appear in records from the sensors about 1 m and 2 m from the source. They are not in Figure 4. They are not continuous background: measured in the quiet interval just before the next hammer strike, where the previous blow's coda has fully decayed, both lines vanish. They are present only in the struck records and decay away between blows, so they are driven by the hammer strike, strongly polarized along the radial direction (79 to 81% of the band energy at 420 Hz and 97 to 98% at 466 Hz in the source-aligned frame). Their cause is not established. By sensor position, the line was at 420 Hz at the 2 m position (morning, no target) and at 466 Hz at the 1 m position, recorded there by two different sensors, one in the morning with no target and one in the afternoon with targets; the farther sensor (about 3 m) never showed either line. On the same hammer blows the 1 m and 2 m sensors ring at different frequencies, and two different sensors agree at 1 m, so the lines most likely belong to the position; they are not the sensor mount. The lines do not divide cleanly by session or by target. We considered the electrical generator that sat approximately 2-meters outside the enclosure, but the instrument digitizes on the sensor and carries only digital data thereafter, leaving no analog signal path for a radiated field to enter; the lines are also absent from the pre-strike quiet, where a continuous source would remain. We report them as real, narrowband features of unknown origin present in a subset of runs.

Because the lines differ between sensor positions, and the no-target and with-target runs were recorded at different positions, they confound the target comparison. Their presence is also a reminder that a before-and-after single-target design cannot fully separate a target effect from changes in the site environment between sessions, which highlights the importance of our plans to use data for analysis as it is acquired by an array of multi-instrumented penetrometers rather than acquire and store it for post processing.

The broad peaks near 372 and 564 Hz at BCDC, strongest about 1 m from the source, have no counterpart at Bally Cliff Farm. These higher-frequency BCDC features therefore appear to be site-specific.

The datasets remain small (at BCDC, one no-target and three with-target runs on the one sensor that recorded both at a fixed position; at Bally Cliff, three no-target versus eleven short with-target runs). A paired trough and peak near 130 Hz appears at both sites only when different recordings are compared: two sensors on two mount types at Bally Cliff, and different sensor positions at BCDC. We therefore report no spectral change at either site that can be cleanly attributed to the targets, and identify a within-session design, recording no-target and with-target data at the same time on an array, as necessary to separate a target effect from other changes between runs.

No effort has been made to develop similar data for SAND or NATIVE SOIL because the Nyquist limit combined with the data acquisition rate of slightly over 300 Hz limits the frequencies that can be detected.

4.8 Detection Limits

Estimating ERW detection limits for seismic technology is an inherently site-specific exercise because the four key values in the estimates; the relevant seismic velocity (P-wave as worst case); seismic wave frequency; the characteristic dimensions of the ERW threat; and the

sensor's view of that threat are all controlled by the hyperlocal conditions and are unknown for any general discussion. Thus, this examination is a single example based on the hyperlocal and very limited test data from the BCDC IPG CLAY test area discussed in Section 4.7.

The CLAY records carry energy near 132 Hz and broad peaks near 372 and 564 Hz, the latter strongest about 1 m from the source. Using the P-wave velocity of 272 m/s (Section 4.3) as an example, we are able to calculate the minimum detectable size for a buried item. These values produce λ/4 minimum detection dimensions [15] of 515, 183, and 121 mm at frequencies where the soil carried measurable energy. These frequencies are used here for illustration; what produces them is not established. The physical mechanism linking spectral perturbation frequency to object dimension requires further investigation.

Lower-velocity shear and surface waves would indicate the ability to detect proportionally smaller targets; a synchronized sensor pair in CLAY has since measured a surface-wave velocity of 159 ± 9 m/s (Gorin et al., in preparation).

Unexploded ordnance dimensions vary greatly. For example, hand grenades might be represented as a small cylinder 64 mm in diameter and 89 mm long. Similar dimensions for a 60 mm mortar shell would be 60x300 mm and for a 155 mm artillery round might be 155x750 mm. The potential for detecting such ERW using the worst-case wavelengths associated with the P-wave velocity is summarized by the "X" in the combined dimension and frequency in this table.

Table 2. Example unexploded ordnance detection limits at frequencies present in the measured soil response.

Typical Ordnance	Short Dimension	Frequency (Hz)			Long Dimension	Frequency (Hz)		
		132	372	564		132	372	564
Grenade	64 mm				89 mm			
60 mm Mortar	60 mm				300 mm		X	X
155 mm Artillery Round	155 mm			X	750 mm	X	X	X

Note that in actual operation, seismic sensors will be placed such that their hemispherical coverage volume overlap (Section 3.2), thus significantly increasing the likelihood that one or more observations will be made of the long dimension.

This illustrative example is from specific, hyperlocal measurements and demonstrates the value of the hyperlocal measurement approach: Every hyperlocal location on every site has its own measured and calculated detection limits.

5 Discussion

5.1 Implications for ERW Clearance Operations

The seismic search technology reported here benefits ERW search operations in multiple ways.

The most significant benefit is the technology's hyperlocal methodology. The specific search process can be adapted to meet the needs of a specific site. Source-sensor equipment spacing can be adjusted to meet small threat detection needs based on measured capabilities rather than set operating standards. Overlapping sensing volumes add to a rich understanding of the subsurface world through different views of a given volume.

The hyperlocal methodology ultimately produces multiple detection opportunities with a single data stream. Buried objects, such as the shovels used at Bally Cliff Farm and BCDC, are expected to reflect or scatter seismic waves and change the frequency response. Measurements of P-wave velocity and attenuation characteristics at hyperlocal scales also examine the soil itself to detect changes in any characteristic—velocity, for example—over a short distance that may be statistically significant. Future testing will evaluate the use of such differences to address both landmine and UXO hazards in a single pass rather than the repeated examinations that are currently required [12].

The adaptive nature of the hyperlocal deployment allows an algorithm-based balancing of detection sensitivity and search productivity. Hyperlocal soil measurements allow optimization of search parameters such as stimulus count, sensor spacing, and search speed for each specific area.

Seismic technology is unaffected by soil magnetic characteristics, making it suited to iron-rich volcanic soils and areas heavily contaminated by ferrous debris such as shrapnel, conditions that severely degrade magnetometer and metal detector performance.

Additionally, the seismic technology as planned has the potential for major enhancements.

The technology itself is designed for robotic, rather than human, deployment. This provides many benefits, the most important of which is removing humans from the danger zone. It also leverages human labor for enhanced productivity and can shorten site search timetables through multi-shift work schedules.

The deployment strategy is compatible with other instruments that use orthogonal physics for detection. Integration of an orthogonal sensing modality is now moving from the conceptual phase to the strawman design phase as described in Section 3.3.

The measurement geometry is compatible with tomographic imaging, which would provide subsurface visualization to support detailed investigation, possibly by an orthogonal technology such as GPR, for Explosive Ordnance Disposal operations. Sensor placement requirements and software enhancements to create tomographic images are in the early evaluation stage.

5.2 Limitations

The research reported here is limited by several factors and should be evaluated bearing them in mind.

The research objectives were limited to hyperlocal soil characterization using seismic waves. There was no intent to use those waves to create images nor was any effort made to do so. This is future work.

The test data is from small sample sizes. For example, the BCDC no-target to with-target comparison at a fixed sensor rests on one no-target and three with-target runs. Many more properly controlled experiments with larger sample sizes are required to demonstrate an operational capability.

Our test logs make the presence of many confounding variables during the exploratory testing at Bally Cliff Farm very clear. These included the irregular use of a sound deadening cover or hat, different sensor-to-soil coupling surrogates, occasional hand damping of test equipment vibration, the distance from the seismic source to the sensor, the presence of a target,

and the target's position. While distance-controlled comparisons addressed the most critical confound, even these were somewhat obscured by the non-homogeneous nature of the soil between the seismic source and the sensor from undocumented artifacts such as tree roots.

DAQ bandwidth is an important limitation. It ranged from a low of somewhat more than 300 Hz for the sensor data acquired through the COTS DAQ to 10 kHz for the data logger used with the contact microphones. This variation in bandwidth is particularly important because having no high-frequency data from SAND or NATIVE SOIL limits seismic frequency extraction and P-wave velocity measurement precision as described in Section 4.2.

Our testing included only one direct P-wave velocity measurement. That was done in the BCDC IPG CLAY facility as a "one off" implementation of the instrument and DAQ combination involved. This only demonstrates the measurement capability, not an integrated capability from a single instrument-DAQ IMU. Data reduction is ongoing to extract seismic P-wave velocity from SAND and NATIVE SOIL using the severely degraded multi-channel sample rates, but this will have only very limited precision.

The ERW simulants used were informal, simply metallic probes such as hand shovels inserted into the ground, rather than a to-scale UXO model or calibrated surrogate. We plan to include calibrated surrogate ERW simulants in future testing.

While the soil conditions in CLAY and SAND are well documented, the soil composition in NATIVE SOIL, at Bally Cliff Farm, and the Brady Residence is only estimated from superficial visual assessments. The importance of collecting data defining the soil's characteristics as ground truth during each test program is a lesson learned.

The no-target spectral characterization described in Section 4.4 pools data taken on both August 7 and August 8. These runs were conducted from two separate instrument installations in the same general area with an estimated location offset of between 1 and 5 m. The Bally Cliff target comparison in Section 4.6, by contrast, uses only August 8 runs for both the no-target reference and the with-target pool, so the comparison is within a single installation and is not affected by the offset between setups. The two-installation pooling in Section 4.4 may introduce path-specific spectral variation that contributes to the run-to-run spread visible in Figure 3.

Both CLAY and SAND have concrete floors below the well-defined soil. What effect this artificial boundary has on the observed spectral features has not been analyzed.

The inter-stimulus timing of approximately 0.5 Hz is not optimized. It has been inconsistent due to manual operation. Establishing both the optimal stimulus frequency to balance signal decay with operational throughput and optimal energy for sensor function at varying distances are open research questions. We plan to use automated stimulus mechanisms in the future, but these are conceptual in nature.

Spatial sampling at intervals shorter than the wavelengths of interest would be required for wavefield imaging techniques such as tomographic inversion. This would require several closely spaced sensors to study a specific area of interest identified during the site survey. Tests to investigate this are planned for future array configurations.

The sensor fusion concepts described briefly in Section 3.3 have been studied in some detail but remain entirely hypothetical. No instruments were included in these tests and testing of the multi-physics convergent framework described in this paper is in the design and planning stage.

5.3 Relationship to Prior Work

We are far from the first to propose seismic technology for ERW detection.

Sabatier and Xiang [5, 6] demonstrated acoustic-to-seismic coupling using airborne sound as the seismic stimulus and laser Doppler vibrometry as the sensor to detect landmine resonances. Donskoy [7] extended this with nonlinear vibro-acoustic methods. Both approaches used forced-frequency excitation and a remote sensor for surface measurement, a sensing approach that can be degraded if the soil is hidden as with vegetation. Our approach differs fundamentally in two ways: broadband impulse excitation and subsurface-coupled sensors that listen to the soil's natural response.

Park, Miller, and Xia [10, 11] exploited Multichannel Analysis of Surface Waves (MASW) by measuring shear-wave velocity and analyzing Rayleigh wave propagation to image the subsurface volume. While the application domain differs, the surface-wave dispersion is a phenomenon future array configurations might exploit. Additional research is needed to evaluate how our hyperlocal processes may exploit these measurements.

Current sensor fusion approaches typically combine electromagnetic phenomena such as magnetometry with electromagnetic induction, or metal detection with GPR. While effective, these fuse sensors that respond to related physical properties. The sensors are different but the physics they exploit is similar. The sensor fusion now being considered for the seismic sensor uses orthogonal physical phenomena and adds soil characterization as an input to fusion, thus conditioning detection criteria on measured local soil conditions.

6 Conclusions

The results of the work described in this paper support hypotheses 1 through 5. Hypothesis 6 remains untested. We measured hyperlocal P-wave velocity satisfactorily over short distances in CLAY as well as seismic frequency content both in CLAY and at Bally Cliff Farm. We were able to use that data to calculate temporal attenuation coefficients, spatial attenuation coefficients, and the smallest detectable object within range. We observed spectral differences between no-target and with-target runs at two independent sites, but none can be cleanly attributed to the targets. The detectable sizes are calculated limits, not field detections.

Our use of broadband impulse excitation produced a variety of soil seismic responses that provide potential ERW detection methodologies, which is relevant to hypothesis six, but we did not measure soil property variations associated with disturbed soil. That final step remains for future work.

Per-axis spectral decomposition, checked sensor by sensor, showed that the near-130 Hz difference at both sites came from comparing different sensors (Bally Cliff) or positions (BCDC). Thus, a target contribution cannot be stated as a firm conclusion.

We detected coherent signal propagation at distances of up to 6 m. Our test setups generally operated at distances from the bang plate to the sensors of 6 m or less, but we did observe a marginal feature at 7 m on one run.

All of this was achieved with inexpensive COTS instrumentation.

Despite these achievements, our results cannot be broadly interpreted. The limits of the work include small sample sizes, only superficial knowledge of the soil involved in two of the four counted soil types, and ad hoc ERW simulants.

The work described is preliminary data, not proof that an instrument system based on seismic technology has a broad operational application.

Thus, significant work remains to be done.

We conclude COTS instrumentation and high-frequency, hyperlocal soil characterization have the potential to become the foundation for an economically viable broadly applicable ERW detection system. “Potential” is, however, insufficient and further research into this technology is needed.

7 Acknowledgments

The authors wish to thank some people who provided the kind of foundational support without which this work would not have been completed. They include:

- **Michael (Mike) and Marta Brady** who generously allowed us to use their property for our first testing. This accommodation informed all our subsequent work in critical, irreplaceable ways.
- **James (Jim) Clifford,** whose gracious invitation to use areas of his Bally Cliff Farm allowed us to develop and refine our test strategies in preparation for more formal testing in Texas.
- **Koya Suto** of Terra Australis Geophysica for his expert review of our description of the seismic methodology used, which substantially strengthened the paper.
- **Brian McHugh** of the Bush Combat Development Complex exhibited infinite patience with an evolving test program plan and changing test schedule and a willingness to do whatever he could to help our on-site operations.
- **Robert (Bob) Vernot** of Nextage LLC for his generous sharing of magnetometry expertise and discussions of potential sensor fusion.
- **Dr. Antonios Kontsos** of Rowan University for his help as we crystalized our initial mixed reality strategy.
- **Jason Kroh** of Strados Labs for his help and support as our instrumentation strategy was brought to fruition.
- **Anthropic**’s Claude Chat and Claude Code Artificial Intelligence tools for data processing pipeline development, technical analysis, and manuscript preparation.

8 DATA AVAILABILITY

All work described in this paper was funded by GoVentures, Inc. or performed without charge by volunteers. The processed data supporting the findings of this study are available from the corresponding author upon reasonable request. The raw data and detailed memoranda describing the test activities are available under non-disclosure agreement.

9 Author Biographies

Barney F. Gorin, PE, is a founder of GoVentures, Inc. He holds an MBA from Canisius University, an MSAE from the University of Notre Dame, and a BSAE from Trine University. With more than 45 years of post-baccalaureate engineering experience spanning spacecraft propulsion, robotics, and systems engineering, his recent work focuses on robotically deployed seismic and magnetic sensing methods for ERW detection. He has authored or co-authored 18 publications on topics including robotic construction, lunar surface operations, and sensor systems. He holds three issued patents with two additional applications pending. (Contact: barneygorin@goventures.biz)

C. Scott Vaughen is an Assistant Professor of Mathematics at Montgomery County Community College in Blue Bell, PA, with over 25 years of community college teaching experience. He holds a Bachelor of Science in Mathematics from the University of Florida and a Master of Science in Mathematics from the University of Mississippi, and teaches courses in differential equations, linear algebra, and multivariable calculus. He developed the seismic data processing and spectral analysis pipeline used in this research by applying his mathematical expertise to the signal processing and computational analysis required. (Contact: csvaughen@gmail.com)

Stephen Morehouse is a retired professional pilot with 60 years of flying experience. He has a BS degree in Mechanical Engineering from Tri-State University. During his 5-year tour in the Air Force, he flew 107 combat missions in the F-100-D aircraft delivering a variety of ordnance. He also flew 450 hours of combat in the OV-10 as a Forward Air Controller. After returning from Vietnam, he instructed for 2 years in a Special Operations Wing before starting a 30-year career with the airlines. Basic material support and fabrication with creative out-of-the-box thinking is his contribution to this endeavor.

Janis L. Tabor is a founder and the President and CEO of GoVentures, Inc. She built a career spanning technology policy, science communications, federal government relations, and strategic consulting. Highlights include serving as Executive Director of the Council for Chemical Research, Director of Government Relations for ASME International, and founder and president of EnergyTrack, Inc. She holds a Bachelor of Arts degree from the University of Maryland and is a lifelong learner with graduate and professional studies at institutions ranging from Hood College to Duke University.

Paul Kirchman is a mechanical systems engineer in Aerospace and Nuclear fields. He provided engineering support to Hubble Space Telescope servicing missions, James Webb Space Telescope (JWST), Geostationary Operational Environmental Satellites (GOES), Tracking Data Relay Satellite System (TDRS), and numerous smaller programs. He is a subject matter expert in finite element analysis and software development using MATLAB, Python, and C.

Joseph T. Kujawski is an experienced engineering leader and current IEEE Congressional Fellow with more than two decades of cross-disciplinary accomplishments spanning space systems, electronics, mission architecture, and technology policy. He has delivered complex projects across government, industry, and academia including contributing core electronics to major NASA missions, leading development of space-based weather instruments, and helping transform organizations through AS9100 certification, strategic growth, and multidisciplinary team building. In the U.S. Senate, he provides technical expertise on space, semiconductor, and emerging technology issues, informing legislation, oversight, and constituent engagement. As an

engineering executive, consultant, and inventor with multiple patents, he has guided R&D efforts, secured significant grant funding, and mentored the next generation of engineers. He holds an MSEE from Rensselaer Polytechnic Institute and a BSEE from the University of Alabama at Birmingham.

Patrick McKenna is an expert in the LabVIEW programming language.

Christopher Kujawski is a rising senior studying Electrical Engineering at Texas A&M University Texarkana campus.

10 References

#	Reference
1	Defense Science Board, "Report of the Defense Science Board Task Force on Unexploded Ordnance." Office of the Under Secretary of Defense for Acquisition, Technology, and Logistics, Washington, DC, 2003.
2	International Campaign to Ban Landmines–Cluster Munition Coalition, Landmine Monitor 2025, 27th annual edition, ICBL-CMC, Geneva, 1 December 2025. Available at the-monitor.org.
3	U.S. Department of State, "To Walk the Earth in Safety," Bureau of Political-Military Affairs, FY2024 edition.
4	Oelze, M.L., O'Brien, W.D., Jr., and Darmody, R.G., "Measurement of Attenuation and Speed of Sound in Soils," Soil Science Society of America Journal, vol. 66, pp. 788-796, May 2002.
5	Sabatier, J.M. and Xiang, N., "An Investigation of Acoustic-to-Seismic Coupling to Detect Buried Antitank Landmines," IEEE Trans. Geoscience and Remote Sensing, vol. 39, pp. 1146-1154, 2001.
6	Xiang, N. and Sabatier, J.M., "An experimental study on antipersonnel landmine detection using acoustic-to-seismic coupling," J. Acoust. Soc. Am., vol. 113, pp. 1333-1341, 2003.
7	Donskoy, D., Ekimov, A., Sedunov, N., and Tsionskiy, M., "Nonlinear seismo-acoustic land mine detection and discrimination," J. Acoust. Soc. Am., vol. 111, pp. 2705-2714, 2002.
8	Zagrai, A., Donskoy, D., and Ekimov, A., "Structural vibrations of buried land mines," J. Acoust. Soc. Am., vol. 118(6), pp. 3619-3628, 2005.
9	Masarik, M.P., Burns, J., Thelen, B.T., Kelly, J., and Havens, T.C., "Enhanced buried UXO detection via GPR/EMI data fusion," Proc. SPIE 9823, Detection and Sensing of Mines, Explosive Objects, and Obscured Targets XXI, 2016.
10	Park, C.B., Miller, R.D., and Xia, J., "Multichannel analysis of surface waves," Geophysics, vol. 64(3), pp. 800-808, 1999.
11	Xia, J., Miller, R.D., and Park, C.B., "Estimation of near-surface shear-wave velocity by inversion of Rayleigh wave," Geophysics, vol. 64, pp. 691-700, 1999.
12	Bruschini, C. et al., "Guidebook on Detection Technologies and Systems for Humanitarian Demining," Geneva International Centre for Humanitarian Demining (GICHD), Geneva, 2006.
13	Daniels, D.J. (ed.), "Ground Penetrating Radar," 2nd edition, IET Radar, Sonar and Navigation Series 15, Institution of Electrical Engineers, London, 2004
14	Gorin, B.F., "Project Pinecone Test Summaries v1.1," GoVentures, Inc. Internal Technical Memorandum, January 2026 (proprietary data requiring a non-disclosure agreement; available from corresponding author upon request).
15	Sheriff, R.E. and Geldart, L.P., "Exploration Seismology," 2nd edition, Cambridge University Press, 1995
16	Gorin, B.F., "Aug 11 Jim's Farm — Mount-Comparison Experiment Analysis," GoVentures, Inc. Internal Technical Memorandum, Rev. 3.0, July 2026 (available from corresponding author upon request).

11 Appendix: Acronyms

Acronym	Meaning
AA	Aluminum Angle (ground coupling bracket)
BCDC	Bush Combat Development Complex (Texas test site)
COTS	Commercial Off The Shelf
DAQ	Data Acquisition system
DC	Direct Current
ERW	Explosive Remnants of War
FFT	Fast Fourier Transform
GPR	Ground Penetrating Radar
IMU	Inertial Measurement Unit
IPG	Innovation Proving Grounds (at BCDC)
MASW	Multichannel Analysis of Surface Waves
MEMS	Microelectromechanical Systems
SC	Sod-Cutter (ground coupling blade)
T/NT	with Target and No-Target run labels
UXO	Unexploded Ordnance